Off-Design Analysis of Axisymmetric External-Compression Supersonic Inlets for Mach 1.4 to 2.0

John W. Slater
John.W.Slater@nasa.gov
NASA John H. Glenn Research Center
Inlets and Nozzles Branch, Propulsion Division
Cleveland, Ohio
USA

ABSTRACT

Supersonic axisymmetric, external-compression inlets designed for freestream Mach numbers of Mach 1.4, 1.7, and 2.0 were evaluated to characterize their off-design performance. The inlets were assumed to be isolated from the airframe with freestream conditions, engine-face geometry, and flow rates established from a reference NASA commercial aircraft concept. The off-design performance was characterized using computational fluid dynamics (CFD) simulations. The study characterized the off-design performance at the cruise condition for variations in the inlet flow rate, angle-of-attack, and freestream Mach number. This included performance at take-off and approach-to-landing conditions for which auxiliary intakes were included. The inlet performance was characterized by the inlet flow ratio, total pressure recovery and distortion, and cowl exterior wave drag. An understanding of the off-design performance of the axisymmetric inlets provides information for the selection of inlets for commercial supersonic aircraft.

Keywords: Supersonic Inlets, Computational Fluid Dynamics

NOMENCLATURE

AL	Approach-to-Landing
BC	Boundary Condition
DPC/P	SAE ARP 1420 circumferential distortion index
DPR/P	SAE ARP 1420 radial distortion index
RSM	Response Surface Method
TO	Take-off

Symbols

A_1, A_{SD}, A_2	Cross-sectional area at the inlet stations
A_{cap}	Reference capture area
α_0	Angle-of-attack
C_{Dwave}	Cowl wave drag coefficient
D_2	Diameter of the engine face
h_0	Altitude
h_1	Height of the inlet cross-section at station 1
L_{inlet}	Length of the inlet
L_{subd}	Length of the subsonic diffuser
M_0	Freestream Mach number
M_2	Engine-face Mach number
p_{t0}	Freestream total pressure
p_{t2}	Average engine-face total pressure
r	Radius
r_{cbsh}	Radius of curvature of the centerbody shoulder
S_{inlet}	Total surface area of the inlet
θ	Angle, slope
T_{t0}	Freestream total temperature
W_2	Engine-face flow rate
W_{bleed}	Flow rate through the bleed slot or region
W_{cap}	Reference capture flow rate
W_{C2}	Engine-face corrected flow rate
W_{C2*}	Engine-face corrected flow rate for the inlet design condition
x, y, z	Cartesian coordinates

1.0 INTRODUCTION

Commercial supersonic flight requires an efficient propulsion system consisting of an inlet, turbofan engine, and nozzle. The inlet captures, conditions, and supplies air to the engine. The inlet, along with the complete propulsion system and aircraft, need to perform in a stable and efficient manner throughout the mission of the aircraft for take-off, climb, cruise, descent, approach, and landing.

A previous study [1] explored the design of several types of external-compression inlets for a NASA concept aircraft [2] at cruise speeds of Mach 1.4, 1.7, and 2.0. The types of inlets included the axisymmetric pitot, axisymmetric spike, two-dimensional single-duct, two-dimensional bifurcated-duct, and streamline-traced inlets. The results provided information on the relative size and the aerodynamic performance of the inlets for the cruise conditions where a commercial aircraft would spend most of its flight. The results suggested that the axisymmetric spike inlet was a leading choice of inlet for Mach 1.4 and 1.7, but that the two-dimensional and streamline-traced inlets provided potential benefits for Mach 1.7 and 2.0.

The focus of this paper is the refinement and characterization of the aerodynamic performance of the axisymmetric spike inlets at off-design conditions. Section 2 includes a description of the freestream and engine face conditions that describe the upstream and downstream boundary conditions for the design and analysis of the inlets. The geometry model for the axisymmetric spike inlets is then described. Section 3 discusses the computational fluid dynamics (CFD) methods used to perform aerodynamic analysis of the airflow through and about the inlets. Section 4 presents the results of the current study. First, the axisymmetric spike inlets for Mach 1.4, 1.7, and 2.0 were refined for the respective cruise conditions using an optimization method based on design-of-experiments (DOE) and response surface modelling (RSM). At the respective cruise conditions, the inlets were analysed for variations in the engine flow rate, angle-of-attack, and freestream Mach number. Second, the inlets were analysed to create performance curves for climb, transonic, and sub-cruise supersonic conditions. Third, the inlets were analysed for take-off and approach-to-landing conditions involving the use of auxiliary intakes.

2.0 DESCRIPTION OF THE INLETS

The inlets are described through the specification of the freestream and engine face conditions along with a geometry model for the components of the inlet.

2.1 Freestream and Engine Face Conditions

The design of an inlet requires the specification of the flow conditions approaching the inlet and the dimensions and flow rates at the engine face, which is the interface of the inlet with the engine. These conditions constitute the upstream and downstream boundary conditions, respectively, for the inlet design problem. Thus, the inlet design problem is dependent on the integration of the inlet with the aircraft and on the selection of the engine and its propulsion cycle.

For the current study, the freestream and engine face conditions were obtained from consideration of the NASA Supersonic Technology Concept Aeroplane (STCA) [2]. The STCA is a 55-ton business-class airplane concept powered by three turbofan engines and designed to perform transatlantic flights with 8 passengers at a cruise of Mach 1.4. The STCA study also included a conceptual design of a low-bypass turbofan engine, which was used for the inlet design studies of this paper.

The flow conditions approaching the inlet can be influenced by the flow about the aircraft and the manner of integration of the inlet with the aircraft. For a commercial supersonic aircraft, an inlet would likely be integrated with aircraft to provide for high efficiency involving minimal distortion of the flow approaching the inlet. Thus, for the current inlet design study, the inlet was considered isolated from the aircraft with freestream conditions specified as the flow conditions approaching the inlet. These conditions are acceptable for the current study since the objective was to compare inlet performance as inlet design factors, freestream conditions, and engine face conditions were varied rather than obtain absolute inlet performance.

The study considered the range of freestream conditions from take-off to cruise. Table 1 lists the discrete freestream Mach numbers at which analyses were performed. Within the inlet flowfield, the Society of Automotive Engineers (SAE) Aerospace Standard (AS) 755 [3] was used to designate quasi-one-dimensional stations. The freestream station was designated with the subscript “0 with the freestream Mach

number is designated as M_0. The take-off, approach-to-landing, climb, transonic, and supersonic conditions are identified in Table 1. For the supersonic freestream conditions, the respective cruise conditions are indicated in Table 1 with the values of M_0 in bold. The mission profile for the STCA aircraft provided the altitude (h_0) for each freestream Mach number. The US Standard Atmosphere model was used to provide the thermodynamic conditions for freestream Mach number, as listed in Table 1. The STCA study [2] only provided mission data up to $M_0 = 1.4$. For the current study, the data was linearly extrapolated to provide data for $1.4 < M_0 \leq 2.0$.

The engine face conditions require specification of the engine face geometry and the engine flow rate. The STCA turbofan engine was based on publicly available data related to the CFM International CFM56-7B engine. The engine has a single-stage fan with a smaller diameter than that of the CFM56, but with a larger pressure ratio. The low-pressure compressor was removed to compensate for the higher ram pressure and temperatures of supersonic flight. For the inlet of this study, the engine face was modelled as an annular cross-section with a hub at its center and oriented to be perpendicular to the x-axis. Per the SAE AS 755 [3] the engine face was designated with a subscript "2". The engine face had a diameter of $D_2 = 3.625$ feet with a hub-to-tip ratio of $D_{hub}/D_2 = 0.3$. For the axisymmetric spike inlets, the hub of the centerbody mated up to the hub of the engine. The cross-sectional area of the engine face (A_2) was formed by the circular engine face and hub diameter and has cross-sectional area of $A_2 = 9.3918$ ft^2. The center of the engine face was positioned on the vertical plane of inlet symmetry (i.e., $z_2 = 0$ ft). The axial placement of the engine face (x_2) depended on the overall length of the inlet. The vertical placement of the engine face (y_2) was coincident with the inlet axis-of-symmetry.

The engine flow rate was specified by the engine-face corrected flow rate (W_{C2}), which was set by the desired level of thrust as part of the mission of the aircraft. The values of the maximum engine-face corrected flow rate used for the inlet design and analysis for each freestream Mach number (M_0) are listed in Table 1. The engine-face corrected flow rate decreased with increased freestream Mach number in response to limits on the engine maximum temperature. Ref. [2] only provides data for the engine of the STCA aircraft up to $M_0 = 1.4$. The values of W_{C2*} listed in Table 1 for $M_0 > 1.4$ were obtained using a linear extrapolation of the STCA engine data for $M_0 = 1.3$ and 1.4. The engine-face corrected flow rate corresponded to an engine-face mass-averaged Mach number (M_2), which are also listed in Table 1. For the Mach 0.4 approach-to-landing condition, the lower value of W_{C2*} corresponds to a throttle setting of 75% of maximum.

Table 1. Freestream and engine face flow conditions.

	M_0	h_0 (ft)	p_{t0} (psi)	T_{t0} (°R)	α (deg)	W_{C2*} (lbm/s)	M_2
Take-Off	0.3	0	15.643	528.01	12	419	0.683
Approach-to-Landing	0.4	5000	13.653	516.87	6	318	0.700
Climb	0.6	20000	8.614	479.56	4	424	0.700
	0.8	35000	5.271	444.27	2	424	0.700
Transonic	0.9	40000	4.600	453.14	0	427	0.711
	1.0	45000	4.049	467.96	0	427	0.711
	1.1	48000	3.954	484.34	0	427	0.711
Supersonic Cruise and Off-Design	1.2	49000	4.280	502.28	0	427	0.711
	1.3	50000	4.661	521.78	0	423	0.696
	1.4	50000	5.353	542.84	0	413	0.663
	1.5	53000	5.346	565.46	0	403	0.634
	1.6	55000	5.622	589.63	0	393	0.606
	1.7	55000	6.529	615.37	0	383	0.581
	1.8	58000	5.346	565.46	0	373	0.557
	1.9	60000	6.970	671.53	0	363	0.535
	2.0	60000	8.139	701.95	0	353	0.514

2.2 Geometry Model for the Axisymmetric Spike Inlets

This study examined the design and analysis of axisymmetric spike inlets as illustrated in Fig. 1, which shows an inlet for Mach 1.7. An axisymmetric spike inlet consists of an axisymmetric centerbody with a conical spike. The centerbody spike and

forward portions of the centerbody form the external supersonic diffuser consisting of one or more stages that at supersonic speeds create an oblique shock and Mach wave system that decelerates and compresses the supersonic flow. The conical spike forms the first stage and has a semi-vertex angle of θ_{stg1} that forms the initial conical, oblique shock wave at the nose of the conical spike, as shown in the schematic of Fig. 1.

The external supersonic diffuser of the inlet of Fig. 1 has three stages. The second stage is a curved segment that forms Mach waves that are focused onto the cowl lip. A method-of-characteristics (MOC) solution is used within SUPIN to establish the coordinates of the second stage. The Mach waves perform isentropic compression through a gradual turning from an angle of θ_{stg1} to θ_{stg3}, which is the angle of the third stage. The second stage could alternatively be conical which would form conical, oblique shock waves at the start of the second and third stages.

The task of the external supersonic diffuser is to decelerate the supersonic flow from the freestream Mach number of M_0 to a Mach number of M_{EX} at the end of the external supersonic diffuser. The value of M_{EX} is the mass-averaged Mach number across the conical surface at the end of the external supersonic diffuser. For the axisymmetric external supersonic diffuser, the Mach number at the end of the external supersonic diffuser increases in the radial direction from the centerbody to the cowl lip. Further, the flow angle decreases from a value of θ_{stg3} at the centerbody to a lower value at the cowl lip. For the current study, the value of M_{EX} was selected as a design factor. A design factor (i.e., variable or parameter) within the inlet geometry model is an input which can be geometric (e.g., length, angle, area ratio) or aerodynamic (e.g., Mach number, static pressure). All the design factors for the inlet establish a set of design factors that are used within the geometry model to define the surfaces of the inlet. With the specification of M_{EX} and focal points of the wave system, the angles and dimensions of the stages of the external supersonic compression were established.

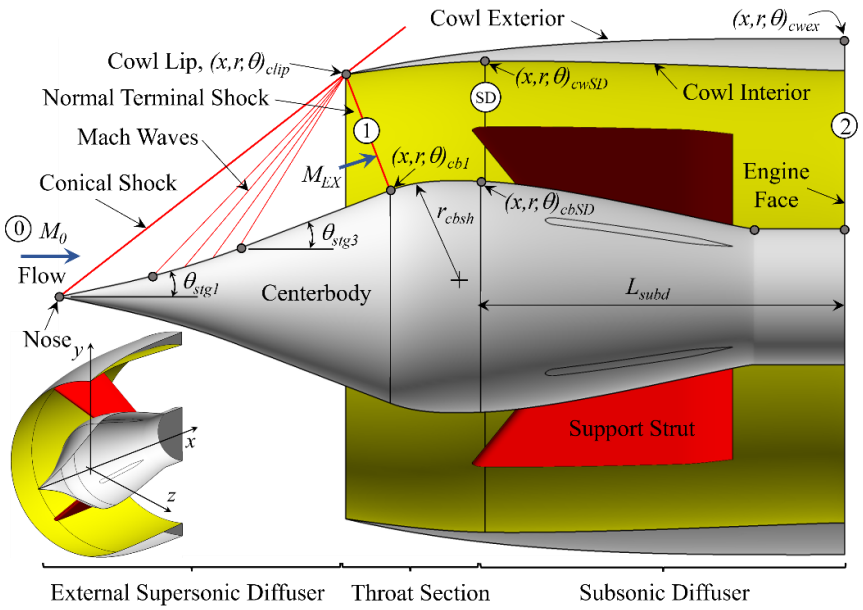

Figure 1. Features and design factors for the axisymmetric spike inlets.

An axisymmetric cowl encloses the inlet. The leading point of the cowl is the cowl lip which is specified with an elliptical profile with very small dimensions to approximate a sharp leading edge to the cowl. For the inlets of this study, the length of the semi-minor axis of the elliptical profile was 0.0005 ft. The aspect ratio of the elliptical profile for the cowl lip was two. The axial coordinate of the cowl lip was specified to be x_{clip} = 0 ft. The radial coordinate of the cowl lip was designated as r_{clip} and was established from the sizing of the inlet capture area (A_{cap}) using the definition of a circular capture area, $A_{cap} = \pi\, r_{clip}^2$. In most cases, the angle of the cowl lip (θ_{clip})

was oriented to match the local flow angle of the external supersonic diffuser flow at the cowl lip.

The cowl consists of the cowl interior and cowl exterior surfaces. The cowl exterior surface starts at the end of the cowl lip exterior with a slope of θ_{clex} that for the inlets of this study were 5 degrees greater than the cowl lip angle (θ_{clip}). The cowl exterior ends at x_{cwex} at a radius of r_{cwex} with an end-slope of θ_{cwex} = 0 degrees.

The cowl lip station is designated with a subscript "1" in accordance with SAE AS 755 [3]. The cowl lip station indicates the start of the internal ducting of the inlet. The planar coordinate on the centerbody at station 1 at the centerbody is $(x,r)_{cb1}$ with a slope matching the last stage of the external supersonic diffuser, $\theta_{cb1} = \theta_{stg3}$, as shown in Fig. 1. The cowl lip station extends between planar coordinates $(x,r)_{cb1}$ to $(x,r)_{clip}$.

The conical first stage of the external supersonic diffuser created a conical shock wave as shown in Fig. 1. The inlets of this study assumed that the conical shock wave was focused onto the cowl lip, which was equivalent to the assumption that the inlets had no supersonic spillage. However, it is common for an inlet to incorporate some supersonic spillage by focusing the conical shock above the cowl lip. This provides some margin against the shock wave impinging onto the inside of the inlet, especially at angle-of-attack, which could degrade the inlet flow and cause instabilities. The assumption of shock wave impingement on the cowl lip was made for the inlets of this study because the interest was on the effects of the design factors and comparison of supersonic inlets rather than design of an inlet for a specific application.

The present study considered external-compression inlets in which a terminal shock wave was positioned across station 1 and took the form of a normal shock wave. Across the terminal shock wave, the supersonic flow at M_{EX} decelerates to a subsonic Mach number of M_1 for entry into the interior ducting of the inlet. A characteristic of an external compression inlet is that excess inlet flow at off-design conditions is allowed to spill out of the inlet at the cowl lip. This requires the terminal shock wave to reposition upstream of station 1 to allow for the spillage of the subsonic flow past the cowl lip.

The forward portion of the interior ducting of the inlet forms the throat section which features curving of the centerbody and cowl interior that turn the subsonic flow toward the engine face. The curved segment of the centerbody is also known as the shoulder. The throat section ends across the conical surface designated as station SD for the start of the subsonic diffuser. The designation "SD" is not specified within SAE AS 755 but introduced to facilitate the geometry model defined for this study. On the centerbody, station SD has the coordinates $(x,r,\theta)_{cbSD}$. The geometry model uses a non-uniform rational B-spline (NURBS) curve to form the profile of the shoulder between points $(x,r,\theta)_{cb1}$ and $(x,r,\theta)_{cbSD}$. The profile was specified to approximate a circular arc with a radius of curvature of r_{cbSD}. Thus, the value of r_{cbSD} was a design factor for the inlets of this study. The value of r_{cbSD} is normalized by the height of the cross-section at station 1 (h_1). The slope θ_{cbSD} was set to be directed along a line extending from point $(x,r)_{cbSD}$ to the hub of the engine face. This was consistent with the task of the throat section of turning the subsonic flow toward the engine face.

The profile of the cowl interior within the throat section was modelled as NURBS curve that extended from the cowl lip point $(x,r,\theta)_{clip}$ to the cowl interior point $(x,r,\theta)_{cwSD}$ at the start of the subsonic diffuser. The coordinates $(x,r)_{cwSD}$ were established using a cross-sectional area A_{SD} determined from the assumption of a linear variation in the subsonic Mach numbers between station 1 (M_1) and the engine face station 2 (M_2). The slope θ_{cwSD} was set to provide for a smooth curve for the cowl interior at station SD.

The aft portion of the internal ducting of the inlet forms the subsonic diffuser that extends between stations SD and the engine-face station 2. The cross-section at station SD is annular and established as part of the design of the throat section. The cross-section at station 2 was established by the engine-face geometry. The primary design factor was the length of the subsonic diffuser (L_{subd}) which is expressed as normalized by the diameter of the engine face (L_{subd}/D_2). Another design aspect of the subsonic

diffuser was then specification of its axial area variation. For the inlets of this study, an axial area variation was imposed that resulted in a linear variation in the quasi-one-dimensional Mach number between stations SD and 2.

The axisymmetric spike inlets required struts to support the centerbody by connecting the centerbody to the cowl. The inlets of this study assumed four struts positioned within the subsonic diffuser and equally spaced about the circumference of the inlet. The struts were clocked to be 45 degrees off the vertical symmetry plane of the inlet. The cross-sections of the struts were defined using a planar definition with an elliptical leading edge, flat sidewalls, and tapered trailing edge with a circular ending. The struts were defined with leading and trailing edge angles specified relative to the *x*-axis in the circumferential plane of the strut. The struts mated to the axisymmetric profiles of the centerbody and cowl interior. The dimensions and angles for the struts were based on reasonable values to keep the struts of minimal size to reduce inlet weight and disturbances to the subsonic flow within the inlet. The struts should provide structural integrity for the inlet; however, no formal structural analysis was performed for this study. Examples of the strut geometry can be seen in Fig. 1.

The struts occupy a portion of the cross-sectional area through the subsonic diffuser. To account for this blockage of the cross-sectional area, the profile of the cowl interior within the subsonic diffuser was adjusted to approximately retain the desired cross-sectional area for linear variation of the Mach number through the subsonic diffuser.

The analysis of the inlet flowfield at take-off and approach-to-landing conditions required the use of auxiliary intakes that allowed flow into the inlet in addition to that flow entering the inlet across station 1. For the axisymmetric spike inlets, the auxiliary intakes were formed by translating the forward portion of the cowl. This approach was investigated in an earlier paper of a Mach 1.4 axisymmetric spike inlet [4]. The auxiliary intakes will be described and illustrated in Section 4 with discussion of the analysis results for the take-off and approach-to-landing conditions.

2.3 NASA Supersonic Inlet Design and Analysis (SUPIN) Tool

The inlets of the current study were modelled and designed using the NASA Supersonic Inlet Design and Analysis (SUPIN) Tool [5]. SUPIN is a FORTRAN 95 program that reads in a text-based input data file that provides the values of the design factors. SUPIN uses the freestream and engine-face conditions along with a set of design factors to size an inlet, estimate the inlet performance, and create the inlet geometry. SUPIN uses compressible flow relations, empirical models, and computational solutions to estimate the quasi-one-dimensional flow properties through the inlet flowpath. The inlet performance is characterized within SUPIN by the inlet flow rates, total pressure recovery at the engine face, and the cowl wave drag. SUPIN generates the surfaces of the inlet and creates a Plot3D file [6] of the surface grid of the inlet. SUPIN can also automatically generate a multi-block, structured grid for a flow domain about the inlet for flow analysis using methods of computational fluid dynamics (CFD). SUPIN is available to US persons through the NASA Software website (software.nasa.gov).

3.0 COMPUTATIONAL METHODS

Methods of computational fluid dynamics (CFD) were used to perform analyses of the aerodynamics of the flow through and about the inlets. The CFD solutions allowed visualization of the flowfield to better understand the shock structures, boundary layers, and other flow features within and about the inlet. From the flowfield, the inlet performance metrics were obtained.

3.1 Wind-US Flow Solver

The Wind-US CFD code [7] was used to solve the steady-state, Reynolds-averaged Navier-Stokes (RANS) equations for the flow properties at the grid points of a multi-block, structured grid for a flow domain about the inlets. Wind-US uses a cell-vertex, finite-volume representation for which the flow solution is located at the grid points and a finite-volume cell is formulated about the grid point. The RANS equations are solved

for the steady-state flow solution using an implicit time-marching algorithm with a first-order, implicit Euler method using local time-stepping. For the simulations presented, the solution process started from freestream conditions specified at all solution points. The simulations were performed assuming calorically perfect air. The inviscid fluxes of the RANS equations were modelled using a second-order, upwind Roe flux-difference splitting method. The flow simulations assumed fully turbulent flow in which the turbulent eddy viscosity was calculated using the two-equation Menter Shear-Stress Transport (SST) turbulence model [8].

3.2 Computational Flow Domain and Boundary Conditions

The flow domain and boundary conditions used for the CFD simulations of the axisymmetric spike inlets are illustrated in Fig. 2. The flow domain shown only includes half of the inlet due to geometric and flowfield symmetry about a vertical plane through the inlet at $z = 0$. The internal and external surfaces of the inlet formed a portion of the boundary of the flow domain where no-slip, adiabatic viscous wall boundary conditions were imposed. The flow domain contained a singular axis upstream of the nose point of the spike. The inflow and farfield boundaries of the flow domain had freestream boundary conditions imposed in which the Mach number, pressure, temperature, and angle-of-attack were specified. For supersonic freestream conditions, the inflow and farfield boundaries were positioned just upstream of the leading-edge oblique shock. For subsonic freestream conditions, the inflow and farfield boundaries were positioned about five engine-face diameters (D_2) forward and away from the inlet, respectively, and uniform freestream conditions were be imposed on those boundaries. Also, for the subsonic simulations, the cowl exterior was extended downstream about two engine-face diameters and a freestream boundary condition was applied. For supersonic speeds, the external outflow boundary was imposed with an extrapolation boundary condition.

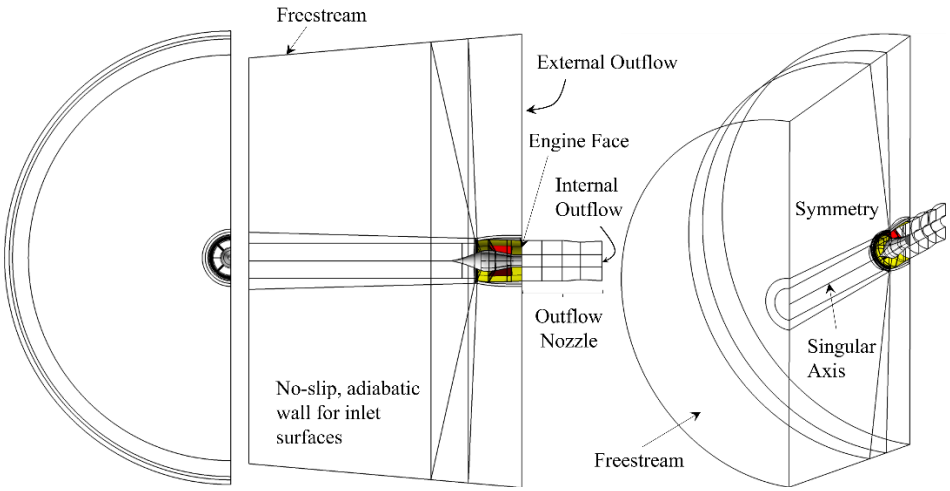

Figure 2. The flow domain and boundary conditions for the CFD simulation of an axisymmetric spike inlet.

Downstream of the engine face, an outflow nozzle section was used to set the flow rate within the inlet. The use of the nozzle section moved the internal outflow boundary condition downstream of the engine face by two engine-face diameters to reduce interference of the flow at the engine face due to the application of the internal outflow boundary condition. The internal outflow boundary condition was set using a converging-diverging nozzle as shown in Fig. 2. The cross-sectional area of the nozzle throat was set by specifying the ratio of the diameter of the nozzle throat to the diameter of the engine-face (D_{noz}/D_2) and was set to form choked flow at the throat. Upstream of the nozzle throat and into the subsonic diffuser, the flow was subsonic and created the necessary backpressure to support the terminal shock about station 1. Reducing the outflow nozzle throat area increased the backpressure, and so reduced the inlet flow rate. Downstream of the outflow nozzle throat, the flow was supersonic, and so, an extrapolation boundary condition could be applied at the internal outflow boundary.

This created a non-reflective, supersonic condition at the internal outflow boundary. The outflow nozzle section was found to create a nearly constant corrected flow rate at the engine face. This allowed for the matching of the design engine-face corrected flow rate for the inlet simulations.

3.3 Computational Grid

The computational grid for the flow domain was generated by dividing the flow domain into multiple blocks and generating structured grids for each block. SUPIN was used to generate the blocks and grid points using an automated process. SUPIN also created the boundary condition file for Wind-US. The inputs to the process include some factors to determine the extents of the flow domain and the resolution of the grid points. The grid resolution factors include the grid resolution of the first grid point away from the wall (Δs_{wall}), the grid resolution within the throat section in the streamwise direction (Δs_{thrt}), and the grid resolution in the circumferential direction at the symmetry boundary (Δs_{sym}). The spacing of the first point off the wall was specified to be Δs_{wall} = 0.00002 ft, which resolved viscous boundary layers to $y^+ < 1$. A grid stretching ratio of 1.15 was used to distribute grid points along the coordinate directions. SUPIN then imposed these grid resolution values along the edges of the inlet geometry and flow domain to compute the required number of grid points along those edges. A grid block topology was assumed for the inlet to form the edges into faces and those faces into blocks. SUPIN generated grids along the edges, on the surfaces, and within the interior volume of each block. The interior block boundaries abutted with other block boundaries. For most blocks, the grid lines matched across block boundaries, but some non-matched boundaries were used to facilitate the structured topology. Figure 3 shows an example of the blocks and grid lines for the block faces on the symmetry boundary. The different colors indicate individual faces of blocks.

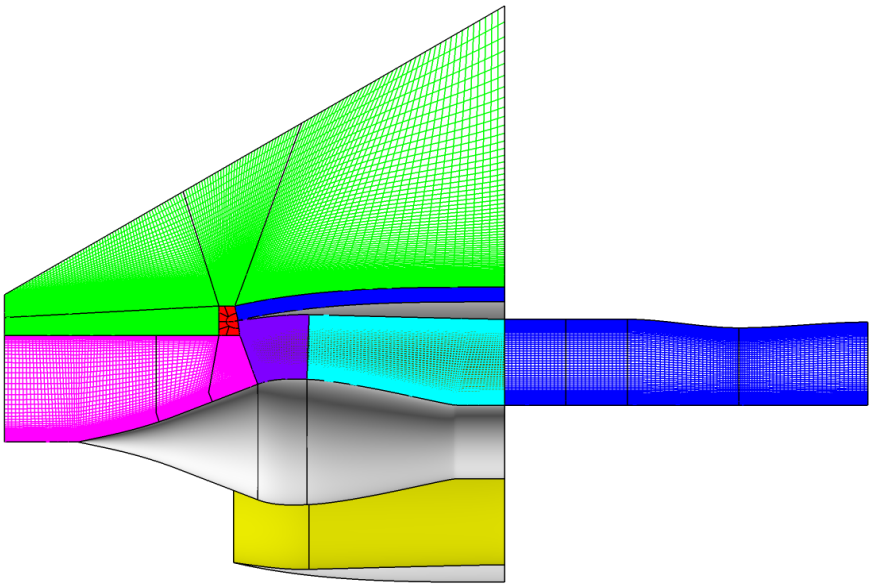

Figure 3. Structured, multi-block, computational grid on the symmetry plane for an axisymmetric spike inlet.

3.4 Inlet Performance Metrics

The first metric of inlet performance was the inlet flow ratio, which was defined as the rate of mass flow passing through the engine face divided by the reference capture flow rate (W_2/W_{cap}). The engine-face flow rate (W_2) was computed from the simulation as the mass-average of the flow through each of the axial grid surfaces through the outflow nozzle section.

The second metric of inlet performance was the inlet total pressure recovery, which was calculated as the mass-averaged total pressure at the engine face divided by the freestream total pressure (p_{t2}/p_{t0}).

The third and fourth metrics of inlet performance were descriptors of the radial and circumferential total pressure distortion at the engine face as represented by the indices DPR/P and DPC/P, respectively. The indices were computed using the methods of the Society of Automotive Engineers (SAE) Aerospace Recommended Practices (ARP) 1420 document [9]. The indices were computed from total pressures interpolated from the CFD simulation onto the probe locations of a virtual 40-probe rake as defined according to the SAE ARP 1420. The rake consisted of eight arms with five probes per rake. The probes were positioned along each arm such that their radial position was at the centroid of equal areas of the annular disk at the engine face.

The fifth metric of inlet performance is the cowl exterior wave drag coefficient (C_{Dwave}). The cowl exterior wave drag is the axial component of the forces due to the static pressure acting on the cowl exterior. The value of C_{Dwave} is this force normalized by the product of the inlet capture area (A_{cap}) and the freestream dynamic pressure (q_0). In general, C_{Dwave} increases as the cowl lip exterior angle (θ_{clex}) and forward-facing area of the cowl exterior increases.

The sixth metric of inlet performance was the total surface area of the inlet (S_{inlet}). This metric was a surrogate for the size and weight of the inlet with the assumption that S_{inlet} increases as the lengths, diameters, and areas of the inlet increases, and the inlet would involve more structure that would increase its weight.

All these metrics are important to the inlet design and analysis and the choice of an optimum inlet requires a compromise in the combination of these performance metrics. For an optimum inlet, a higher total pressure recovery, lower cowl exterior wave drag coefficient, and lower distortion are considered desirable. In addition, a smaller inlet is desirable because length and surface area of the inlet can be correlated to weight. A higher weight inlet will require greater lift and thrust from the aircraft.

One approach for representing the relative effect of these performance metrics is to relate changes in the values of these metrics to change in range of the aircraft. Such a study was conducted as part of the American supersonic transport (SST) project of the late 1960s and early 1970s [10]. That aircraft was intended for Mach 2.7 cruise with a mixed-compression inlet providing airflow to an afterburning turbojet engine. The aircraft was expected to have a nominal range of 3900 miles. The study of Ref. 10 also accounted for the level of inlet bleed as a performance metric; however, the inlets of the current study assumed no bleed. The expected changes in range due to the changes in the total pressure recovery, wave drag, and weight of the inlet are listed in Table 2. It is valid to question whether these data apply to a Mach 1.4, 1.7, or 2.0 aircraft using an external-compression inlet providing airflow to a non-afterburning turbofan engine. Certainly, an updated study of the effect of these inlet performance metrics is warranted. However, it was assumed that the data of Table 2 provided a relative effect of the performance metrics and was useful for the optimization of the inlets of this study. The change in the metrics was made with respect to a reference inlet and here we consider reference values from the modelling and simulation of the Mach 1.7 Gulfstream / NASA Low-Boom Single-Stream (LBSS) inlet [11]. Reference values of the performance metrics were obtained from the modelling of the LBSS inlet within SUPIN and simulation of the inlet using CFD. The reference values for the respective performance metrics are listed in Table 2.

Table 2. Effect of inlet performance metrics on aircraft range.

	p_{t2}/p_{t0}	C_{Dwave}	*Weight*
Metric Δ	-0.01	0.01	0.10
Range Δ	-32	-41	-17
LBSS	0.9470	0.0930	16.64

The overall aircraft range increment (ΔR) is expressed as a sum of change in range increments due to the three performance metrics listed in Table 2,

$$\Delta R = \Delta R_R + \Delta R_D + \Delta R_W \quad (1)$$

where ΔR_R, ΔR_D, and ΔR_W, are the range increments due to the inlet total pressure recovery, wave drag, and weight, respectively. The better inlet was that inlet with the larger value of ΔR. The increments were calculated as,

$$\Delta R_R = \left[\frac{p_{t2}}{p_{t0}} - \left(\frac{p_{t2}}{p_{t0}} \right)_{Ref} \right] \left(\frac{-32}{-0.01} \right) \tag{2}$$

$$\Delta R_D = \left[C_{Dwave} - (C_{Dwave})_{Ref} \right] \left(\frac{-41}{0.01} \right) \tag{3}$$

and

$$\Delta R_W = \left[\frac{\frac{S_{inlet}}{A_{cap}} - \left(\frac{S_{inlet}}{A_{cap}} \right)_{Ref}}{\left(\frac{S_{inlet}}{A_{cap}} \right)_{Ref}} \right] \left(\frac{-17}{0.10} \right) \tag{4}$$

3.5 Iterative Convergence

Iterative convergence of each flow simulation was evaluated through monitoring the convergence of the inlet flow rate, total pressure recovery and distortion. The steady-state solution was considered converged when these values varied less than 0.01% of their values over hundreds of iterations. The solution residuals were also monitored to check that they reduced and approached steady-state values.

4.0 RESULTS

An optimization process was applied to the design of the axisymmetric spike inlets. Performance curves were established for conditions involving take-off, climb, transonic, low supersonic, cruise, and approach-to-landing. At the take-off and approach-to-landing, auxiliary intakes were employed to provide for additional airflow to the engine.

4.1 Axisymmetric Spike Inlet Optimization and Performance at Cruise

A refinement and optimization of three axisymmetric spike inlets for the respective cruise conditions of M_0 = 1.4, 1.7, and 2.0 was performed using methods of design-of-experiments (DOE) and response surface modeling (RSM) [12]. The geometry model described in Section 2 fully described the inlet geometry using three design factors: 1) the mass-averaged Mach number at the end of the external supersonic diffuser (M_{EX}), 2) the normalized radius of curvature for the centerbody shoulder (r_{cbsh}/h_1), and 3) the normalized length of the subsonic diffuser (L_{subd}/D_2). For each of these three design factors, three levels were selected for each respective freestream Mach number based on some previous design exercises with the inlets. Table 3 lists the values of the design factors for the respective values of M_0. In selecting the levels of M_{EX}, one consideration was to avoid values of M_{EX} that would result in boundary layer separation at the foot of the terminal shock at the centerbody surface.

Table 3. Variations of the design factors for the DOE study.

M_0	Design Factor Values									Final Design Factor Values			
	M_{EX}			r_{cbsh} / h_1			L_{subd}/D_2			A_{cap}	M_{EX}	r_{cbsh} / h_1	L_{subd}/D_2
1.4	1.26	1.29	1.32	0.8	1.0	1.2	0.4	0.6	0.8	9.15	1.2825	1.2	0.5
1.7	1.30	1.34	1.38	2.0	3.0	4.0	0.4	0.7	1.0	9.96	1.38	1.0	0.8
2.0	1.30	1.34	1.38	1.0	2.0	3.0	0.8	1.0	1.2	11.47	1.38	1.5	1.0

The DOE study for each inlet used a central-composite-face-centered (CCF) statistical design [12] that required 15 inlet configurations and CFD simulations. The simulations were performed for a planar, axisymmetric flow domain. For each inlet configuration, SUPIN was used to generate the geometry and CFD grid. As part of the CFD simulation for each inlet configuration, the capture area (A_{cap}) was adjusted to yield minimal subsonic spillage past the cowl lip and the outflow nozzle throat setting (D_{noz}/D_2) was adjusted so that the inlet engine face conditions matched the desired corrected flow rate (W_{C2}) listed in Table 1. Thus, usually three to eight CFD

simulations were required for each desired inlet configuration until the proper values of A_{cap} and D_{noz}/D_2 were achieved. Once the desired CFD simulation for the inlet configuration was completed, the performance metrics were computed and the range increment (ΔR) was calculated using Eqs. 1 to 4. The value of ΔR served as the response variable for the response surface modeling (RSM).

Once all CFD simulations were completed for the fifteen inlet configurations, a statistical analysis was performed using RSM. The objective of the RSM was to determine the significance of each of the three factors and build a surrogate model for the value of range increment (ΔR) as a function of the statistically significant design factors. For the CCF, the response model was at most a quadratic polynomial. From the model, it was possible to determine an optimum set of design factors.

The results of the RSM for each inlet is summarized in Table 4 showing the *F*-statistics from the analysis-of-variance (ANOVA) from the RSM for each inlet. Values of the *F*-statistic greater than 5.0 indicate that the model and individual factors are statistically significant [12]. For the $M_0 = 1.4$ inlet, a model could not be built due to the noise within the values of the response variable, ΔR. In other words, the statistical analysis could not establish that the variations in ΔR were directly the result of changes in the design factors.

Table 4. *F*-statistics from the analysis-of-variance of the RSM for each inlet.

M_0	M_{EX}	r_{cbsh} / h_1	L_{subd}/D_2	Model Form
1.4	-	-	-	-
1.7	147	149	-	Linear
2.0	1221	4827	17	Quadratic

For the $M_0 = 1.7$ inlet, a linear model was possible with the design factors M_{EX} and r_{cbsh}/h_1 being roughly equally significant. The effect of the design factors can also be illustrated through the plots of ΔR for each of the design factors, as shown in Fig. 4. The top left plot shows a distinct trend that ΔR increased as M_{EX} increased. The top right plot shows that ΔR increased as r_{cbsh}/h_1 decreased. The bottom left plot indicates that ΔR has little change with variation in L_{subd}/D_2. The variation in the components of ΔR is illustrated in the bottom right plots of Fig. 4. Of the 15 simulations for the $M_0 = 1.7$ inlet, the values of the range increment varied from a low of $\Delta R = -206$ to a high of 69.5, which was obtained with $M_{EX} = 1.38$, $r_{cbsh}/h_1 = 2.0$, and $L_{subd}/D_2 = 1.0$. The plot with the filled circles labeled "Total" shows this variation. In examining the variations of component range increments, the cowl wave drag component shows the greatest range in variation, and so made a large impact on the values of ΔR.

For the $M_0 = 2.0$ inlet, a quadratic model was possible with all three of the design factors being considered significant. The design factor r_{cbsh}/h_1 was more significant than M_{EX} and L_{subd}/D_2 was less significant. Once the DOE and RSM were completed for the inlets, it was determined that the geometry model considerably changed the shaping of the cowl exterior when r_{cbsh}/h_1 was changed. This led to perhaps too great a change in the cowl wave drag. A task for future design studies is to alter the geometry model to lessen the effect of r_{cbsh}/h_1 on the shape of the cowl exterior.

The results of the DOE and RSM studies were taken into consideration for the selection of the final values of the design factors for the respective inlets, which are listed in Table 3. While optimum values of the design factors were obtained from the RSM polynomial models, the final sets of design factors and final inlet configurations were refined through additional CFD simulations. The value of $M_{EX} = 1.2825$ for the $M_0 = 1.4$ inlet reflects that the slope of the single-stage external supersonic diffuser was adjusted to mate to a constant diameter centerbody. For the $M_0 = 1.7$ inlet, the subsonic diffuser was altered to include a constant-diameter aft segment for the centerbody to facilitate a translating centerbody. For all the inlets, the cowl exteriors were refined to reduce cowl wave drag. Also listed in Table 3 are the values of A_{cap} for the inlets.

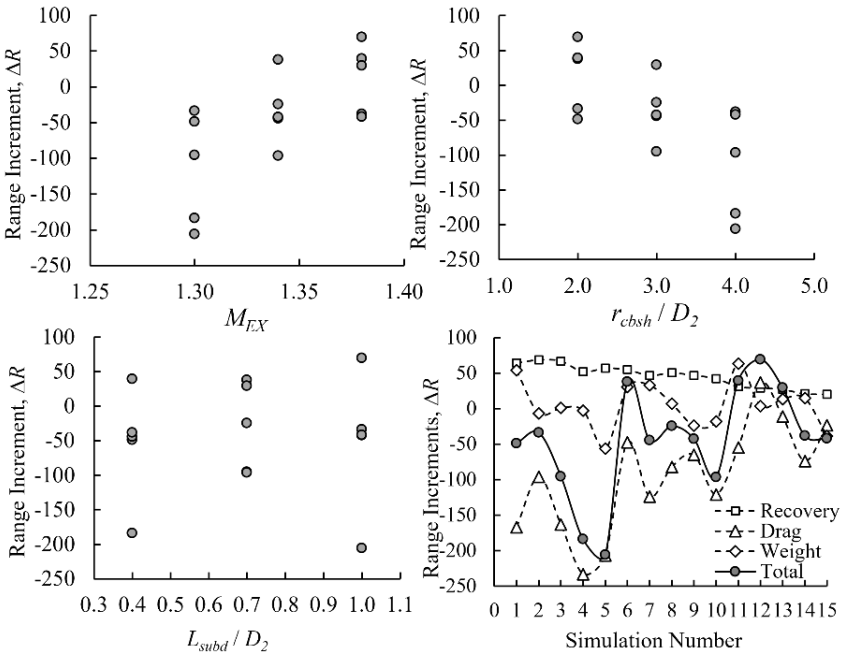

Figure 4. Range increments for the design factors and contributions to the range increments due to responses for the Mach 1.7 inlet optimization.

The final inlet designs are illustrated by the images of Fig. 5. An axisymmetric pitot inlet for M_0 = 1.4 was included as a reference inlet for comparison in sizing and performance. As can be seen, as M_0 increases, the amount of turning of the external supersonic diffuser, slopes of the cowl exterior, and lengths of the inlets increase. Images of the Mach number contours on the symmetry plane from the CFD simulations at the cruise condition for each of the inlets are shown in Fig. 6. The Mach contours show the normal terminal shock right at the cowl lip as desired for minimal subsonic spillage at the design cruise condition. The increased turning of the centerbody with higher values of M_0 results in greater adverse effects on the boundary layer as indicated by the blue shading of the Mach number contours that indicates lower momentum flow within the boundary layer.

The performance metrics from both SUPIN and the CFD simulations are listed in Table 5. The results show generally good comparison between the results from SUPIN and CFD. Differences in cowl wave drag and inlet total pressure recovery increase as M_0 increases. The column in Table 5 with the heading "Mil" lists the expected inlet total pressure recoveries based on the freestream Mach number (M_0) as listed in the Mil-Ref. [13]. This Mil value of inlet total pressure recovery is considered a reasonable goal for an inlet design. All three of the axisymmetric spike inlets designed for this study exceeded the Mil values.

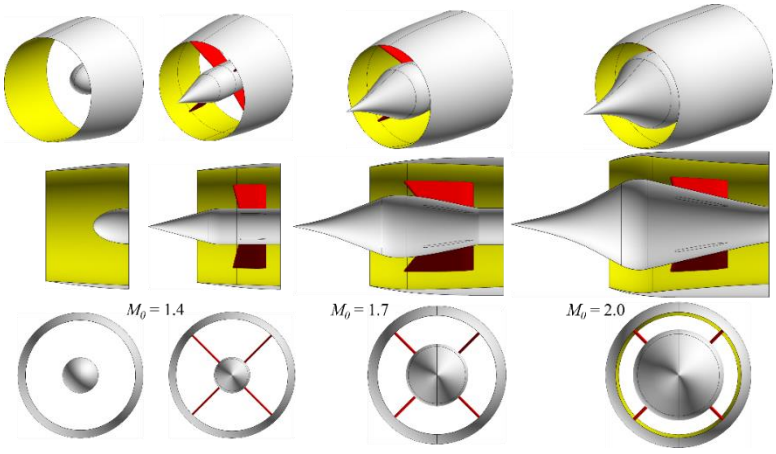

Figure 5. Inlets studied for off-design characterization.

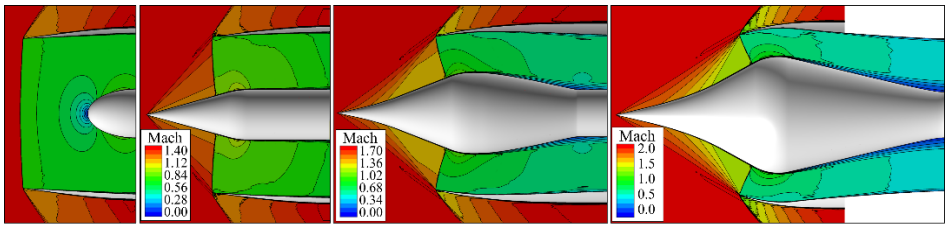

Figure 6. Mach number contours on the symmetry plane for the inlets at their cruise Mach numbers and critical operating conditions.

Table 5. Performance metrics for the inlets at the cruise design condition.

M_0	ft^2	SUPIN				Mil	CFD			
	A_{cap}	W_2/W_{cap}	M_2	C_{Dwave}	p_{t2}/p_{t0}	p_{t2}/p_{t0}	W_2/W_{cap}	M_2	C_{Dwave}	p_{t2}/p_{t0}
1.4	9.15	1.000	0.667	0.0442	0.979	0.973	0.993	0.667	0.0451	0.976
1.7	9.96	1.000	0.582	0.0611	0.960	0.949	0.995	0.584	0.0630	0.955
2.0	11.47	1.000	0.509	0.0859	0.958	0.920	0.991	0.518	0.0978	0.944

4.2 Inlet Performance at Cruise with Variation of the Inlet Flow Ratio

The behaviour of the inlets at cruise conditions as the inlet flow ratio (W_2/W_{cap}) is varied is an important characteristic of the inlets. The inlet flow ratio varies due to variation in the engine throttle due to operation of the aircraft. The behaviour is illustrated by the characteristic curves of the total pressure recovery (p_{t2}/p_{t0}) and SAE indices for the radial (DPR/P) and circumferential (DPC/P) distortion. The characteristic curves for the total pressure recovery and radial distortion indices for the M_0 = 1.4, 1.7, and 2.0 axisymmetric spike inlets are shown in Fig. 7. The points on the curves that are filled indicate the simulation points near the critical operating point of the inlets in which the engine-face corrected flow rate (W_{C2}) was very close the design value of W_{C2*} listed in Table 1. A desired operating point for the inlet at cruise is the critical point where the flow rate and total pressure recovery are at their higher values. For the critical flow conditions, the terminal shock wave structure corresponded to that as shown in Fig. 6.

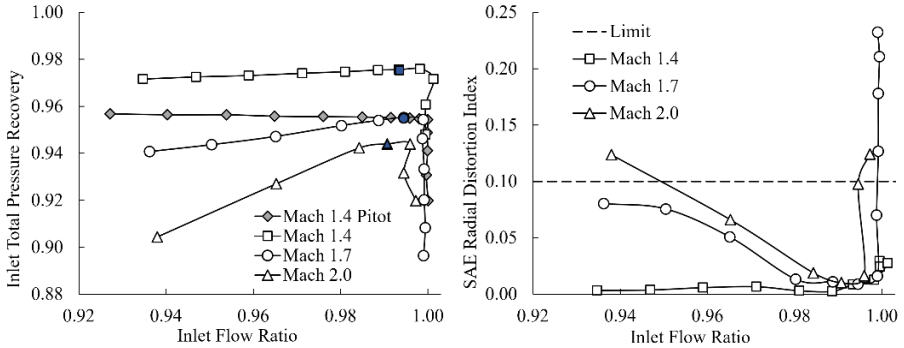

Figure 7. Characteristic curves for the inlet total pressure recovery (left) and radial distortion (right) for the inlets.

The segments of the curves to the left of the critical points are the subcritical legs of the curves in which the corrected flow rate is lower than the critical corrected flow rate. This would correspond to a reduced throttle setting. For these subcritical operating conditions, the inlet is less able to accept the captured flow, and so flow is spilled past the cowl lip. This requires the terminal shock to move upstream of station 1 to allow the subsonic spillage. Such a condition is illustrated by the top image of Fig. 8 for the M_0 = 1.7 inlet and the top image of Fig. 9 for the M_0 = 2.0 inlet.

The segments of the curves to the right of the critical points are the supercritical legs in which the corrected flow rate is greater than the critical corrected flow rate. For these supercritical operating conditions, the terminal shock is drawn into the inlet, as illustrated by the bottom image of Fig. 8 for the M_0 = 1.7 inlet and the bottom image of Fig. 9 for the M_0 = 2.0 inlet. With supersonic inflow into the inlet, the flow rate through station 1 remains constant during the supercritical legs. With no bleed within

the inlet, the engine flow rate also remains constant, as indicated for these inlets by the vertical supercritical legs for the curves. The decrease in total pressure recovery is due to greater losses through the terminal shock structure.

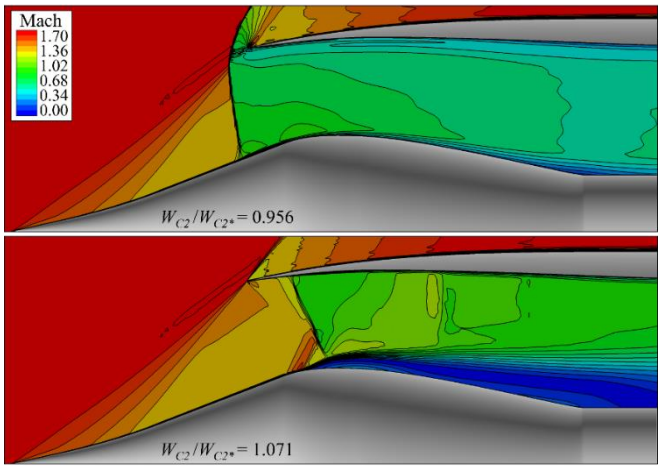

Figure 8. Mach number contours on the symmetry plane for the Mach 1.7 inlet at its most subcritical (top) and supercritical (bottom) simulation conditions.

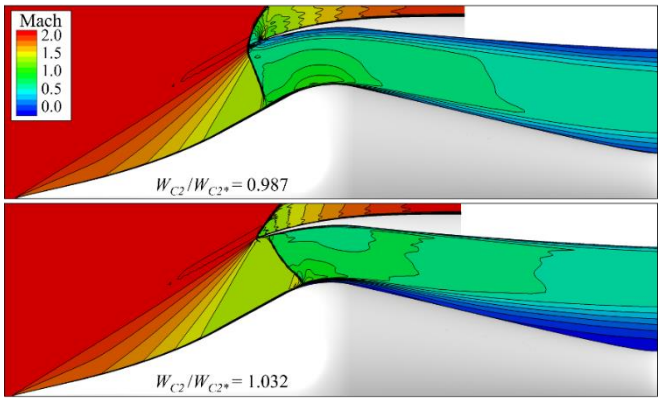

Figure 9. Mach number contours on the symmetry plane for the Mach 2.0 inlet at its most subcritical (top) and supercritical (bottom) simulation conditions.

The characteristic curves for the total pressure recoveries shown in Fig. 7 show that as M_0 increases, the total pressure recoveries decrease due to greater losses through the shock system and dissipation by increasingly adverse boundary layer conditions within the inlet. Included in Fig. 7 is the characteristic curve of the inlet total pressure recoveries for the M_0 = 1.4 axisymmetric pitot inlet. The total pressure recoveries for the subcritical segment of that curve remain at a steady value and are close to the total pressure ratio across a normal shock of p_{t2}/p_{t0} = 0.958. The subcritical total pressure recoveries for the M_0 = 1.4 axisymmetric spike inlet are greater than those for the axisymmetric pitot inlet due to lower total pressure losses through the conical shock wave from the centerbody spike.

Another observation from the characteristic curves for total pressure recoveries was that, as M_0 increased, the slope of subcritical segments of the curves increased. For the M_0 = 2.0 inlet, the slope was considerable such that the peak total pressure recovery of p_{t2}/p_{t0} = 0.944 was only achieved for a small range of engine flow ratios of 0.984 < W_2/W_{cap} < 0.996 about the critical operating point. For the subcritical operation of the M_0 = 2.0 inlet, the terminal shock wave was pushed further upstream as the inlet flow ratio decreased to allow for greater levels of subsonic spillage past the cowl lip. The decrease in the inlet total pressure recovery was due in part to the higher Mach numbers upstream of the terminal shock wave as the terminal shock wave moved upstream. Another contributor to the decrease in the inlet total pressure recovery was the increased interactions of the terminal shock wave with the leading conical shock wave. These

interactions resulted in the formation of a slip surface that was ingested into the inlet, which degraded the flow at the cowl interior.

The use of porous bleed regions on the centerbody in the vicinity of station 1 was investigated as a means for limiting the upstream travel of the terminal shock wave during subcritical inlet operation. The intent of the bleed region is to extract any excess inlet flow to avoid the need for subsonic spillage past the cowl lip that results in the terminal shock wave moving upstream. The placement of a bleed region on the centerbody downstream of station 1 was found to be ineffective. The placement of a bleed region on the centerbody both upstream and downstream of station 1 was found to be reduce the upstream travel of the terminal shock wave and limit losses in the inlet total pressure recovery. This approach resulted in levels of bleed of about 2-3% of the captured inlet flow. The study of the use of bleed is incomplete but will be investigated further in future efforts.

The plots of the right-hand-side of Fig. 7 show the characteristic curves for the SAE radial total pressure distortion index (DPR/P). Values of DPR/P < 0.1 are considered acceptable radial distortion at the engine face [14]. Values of DPR/P ≤ 0.03 and DPC/P < 0.06 are reasonable goals at the critical operating conditions for inlets for commercial supersonic aircraft [15]. The curves of Fig. 7 show very low radial distortion about the critical conditions for all the inlets. Radial distortion increases and exceeds the limits in the extreme supercritical operating conditions. Radial distortion increases in the subcritical operating conditions for the Mach 1.7 and 2.0 inlets. For these inlets, the circumferential total pressure distortion indices (DPC/P) were well below the limits for all flow conditions.

4.3 Inlet Performance at Cruise for Off-Design Conditions

The performance of the axisymmetric spike inlets was examined at their respective cruise Mach numbers for off-design conditions involving variations in the angles-of-attack and freestream Mach number. CFD simulations were performed for angles-of-attack of α_0 = 1, 2, 3, 4, and 5 degrees. CFD simulations were also performed with freestream Mach number variations of $\Delta M_0 = \pm 0.05$ and ± 0.10 relative to the respective cruise Mach numbers and with $\alpha_0 = 0$ degrees. Such variations are expected to occur during cruise due to aircraft or atmospheric perturbations. All CFD simulations were performed while keeping the respective outflow nozzle settings to those for the critical inlet operation at the respective cruise condition.

The characteristic curves for the M_0 = 1.4, 1.7, and 2.0 axisymmetric spike inlets for the variations in angle-of-attack and freestream Mach number are shown in Figs. 10, 11, and 12, respectively. The changes in inlet flow ratios and total pressure recoveries for the variations in angles-of-attack follow a constant-corrected-flow line. The changes for variations in freestream Mach number show a greater level of change than those for variations in angle-of-attack. The radial distortion indices are below the limit for variations in angles-of-attack, however, the limit is exceeded for overspeed conditions of $\Delta M_0 = 0.10$. The circumferential distortion indices were all well below the limit.

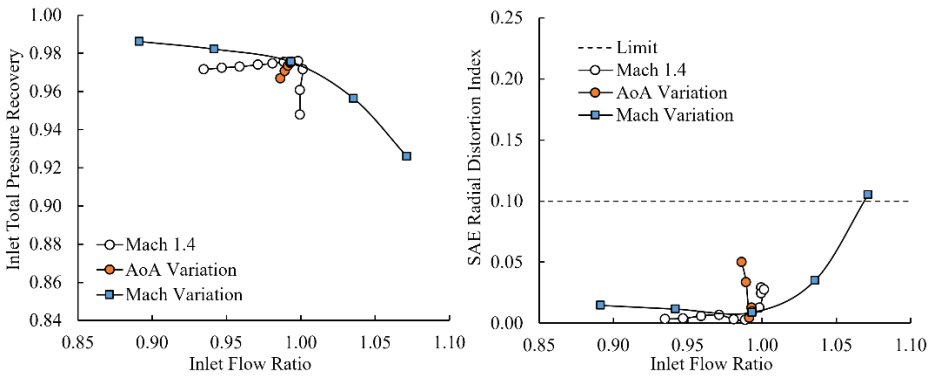

Figure 10. Characteristic curves for the variations in angle-of-attack and Mach number about the cruise condition for the Mach 1.4 inlet.

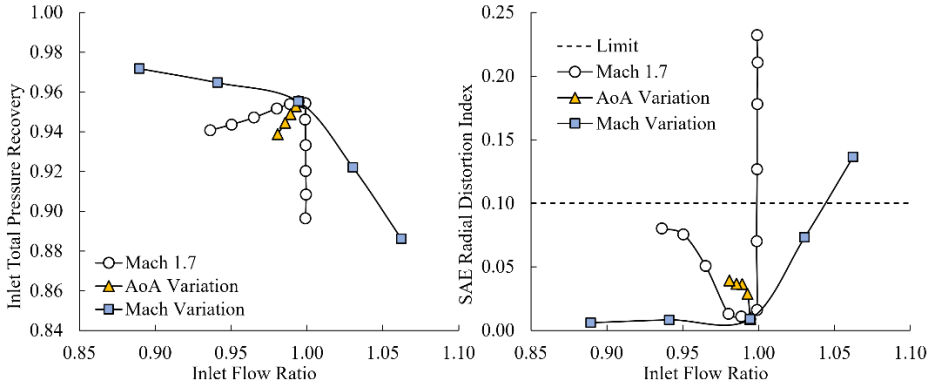

Figure 11. Characteristic curves for the variations in angle-of-attack and Mach number about the cruise condition for the Mach 1.7 inlet.

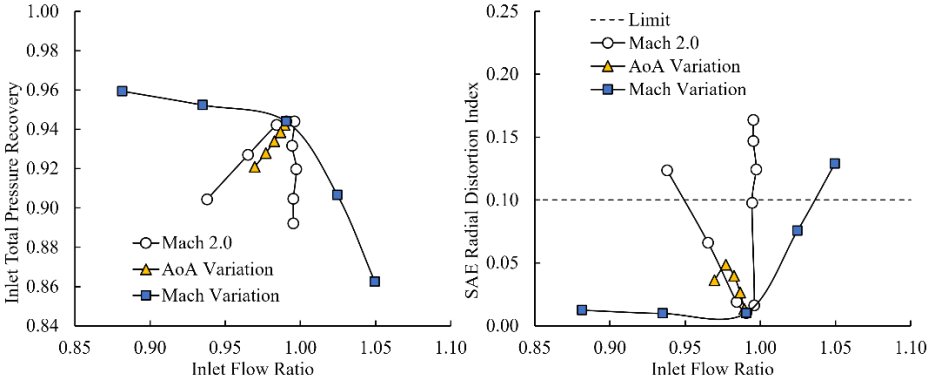

Figure 12. Characteristic curves for the variations in angle-of-attack and Mach number about the cruise condition for the Mach 2.0 inlet.

The Mach number contours on the symmetry plane and at axial stations through the inlets from CFD simulations of the M_0 = 1.4, 1.7, and 2.0 axisymmetric spike inlets at angle-of-attack of α_0 = 5 degrees are shown in Figs. 13, 14, and 15, respectively. On the windward side of the inlet, the terminal shock is drawn into the inlet and causes low-momentum flow to be generated at the cowl interior. For M_0 = 2.0, low-momentum flow is generated on the centerbody due to higher Mach numbers and greater turning about the centerbody shoulder. On the leeward side of the inlet, the terminal shock is pushed ahead of the cowl lip and the flow within the inlet is less degraded than on the windward side.

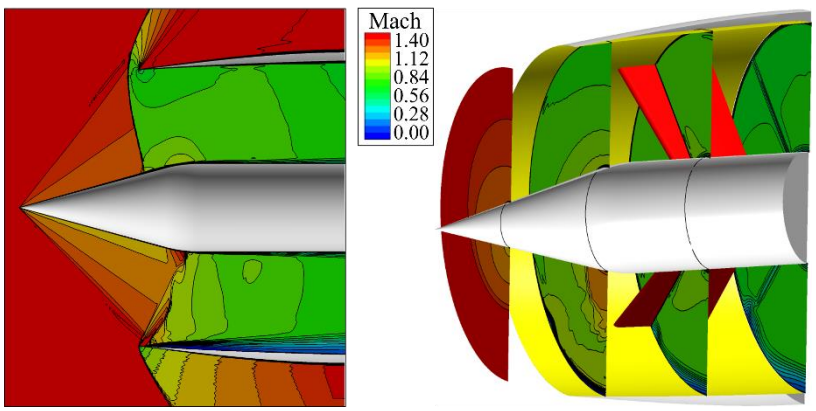

Figure 13. Mach number contours on the symmetry plane (left) and at axial planes (right) from a CFD simulation of the Mach 1.4 inlet at the M_0 = 1.4 cruise conditions and at an angle-of-attack of α_0 = 5 degrees.

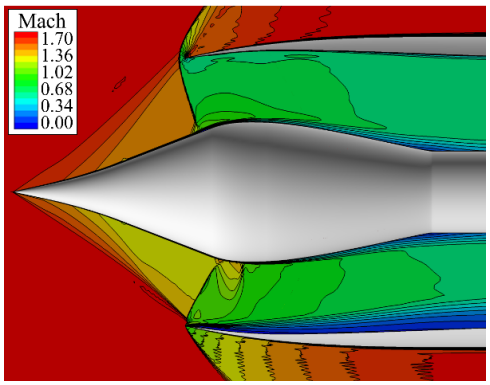

Figure 14. Mach number contours on the symmetry plane from a CFD simulation of the Mach 1.7 inlet at the M_0 = 1.7 cruise conditions and at an angle-of-attack of α_0 = 5 degrees.

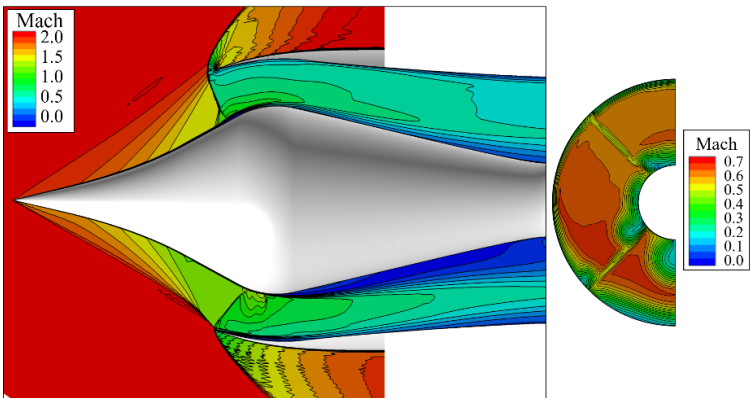

Figure 15. Mach number contours on the symmetry plane (left) and engine-face (right) from a CFD simulation of the Mach 2.0 inlet at the M_0 = 2.0 cruise conditions and at an angle-of-attack of α_0 = 5 degrees.

4.4 Inlet Performance at Off-Design Mach Numbers

The inlets are required to perform in an efficient and stable manner for all freestream Mach numbers from take-off through cruise. The current study involved performing CFD simulations of the inlet flowfields at freestream Mach numbers ranging from M_0 = 0.6 to the respective cruise Mach numbers. For each freestream Mach number, the characteristic curves for inlet total pressure recovery and distortion indices were obtained. Such curves can be used in propulsion system study to understand the operation and performance of the propulsion system over the Mach number range of an aircraft mission.

The plots of Figs. 16, 17, and 18 show the characteristic curves for the inlet total pressure recoveries and SAE radial distortion indices for the respective off-design Mach numbers. For each characteristic curve, the inlet flow rate was normalized using the capture flow rate (W_{cap}) calculated for the respective value of M_0. The general trend is that as M_0 decreases, the inlet total pressures increase. About the transonic range from $0.9 \leq M_0 \leq 1.2$, the characteristic curves are similar and show a limit to the flow that the inlet can capture. The radial distortion indices are well below the limit of DPR/P = 0.1, except at the most supercritical operating conditions, which should be avoided in the operation of the inlets.

It is possible to extract an operating curve across the Mach number range for each of the inlets from the data of Figs. 16, 17, and 18 by connecting likely operating points from the characteristic curves for each M_0. Such operating curves are shown in Fig. 19. The selected points were those on the characteristic curves in which both the recovery and inlet flow ratios were near their maximums. The plots on the left-hand-side of Fig. 19 show the corresponding ratio of the corrected flow rates and would roughly

correspond to a throttle ratio for the engine. The plots show that the M_0 = 2.0 inlet would likely have to operate at reduced throttle at the off-design Mach numbers to avoid choking of the flow within the throat section of the inlet. The plots in the middle of Fig. 19 indicate that the total pressure recoveries of the M_0 = 1.4 and 1.7 inlets are similar for the off-design Mach numbers and those for the M_0 = 2.0 inlet are lower. The plots on the right-hand-side of Fig. 19 indicate that the SAE radial distortion indices are well below the limit across the chosen operating curves. The operating points for M_0 = 0.3 and 0.4 will be discussed in the next subsection.

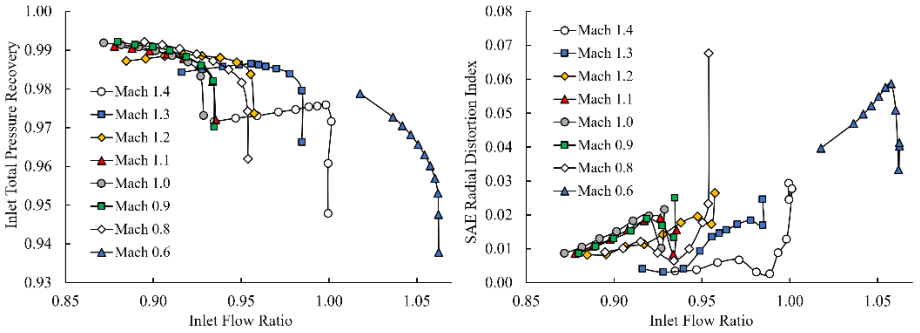

Figure 16. Characteristic curves for total pressure recovery and radial distortion for the Mach 1.4 inlet across the Mach number range from M_0 = 0.6 to 1.4.

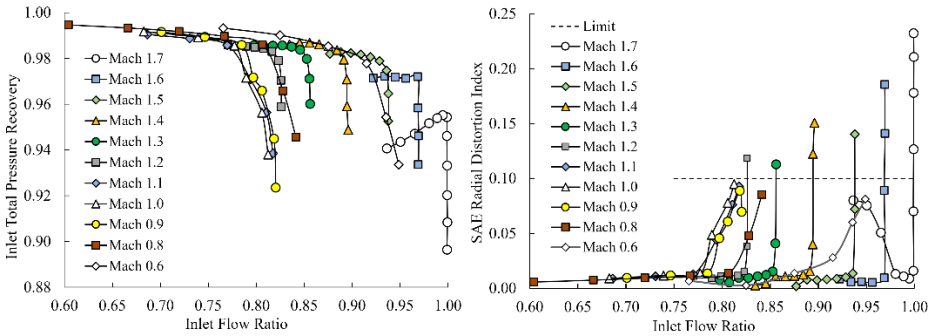

Figure 17. Characteristic curves for total pressure recovery and radial distortion for the Mach 1.7 inlet across the Mach number range from M_0 = 0.6 to 1.7.

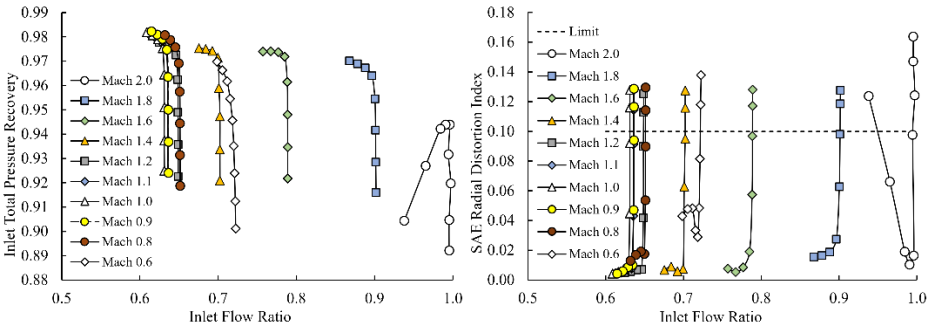

Figure 18. Characteristic curves for total pressure recovery and radial distortion for the Mach 2.0 inlet across the Mach number range from M_0 = 0.6 to 2.0.

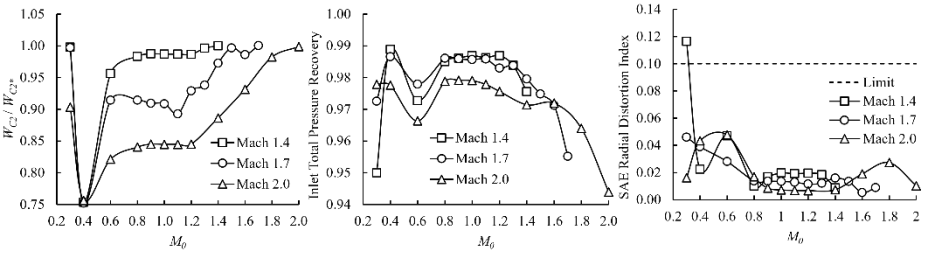

Figure 19. Curves of possible operating points for the inlets across the Mach number range from M_0 = 0.6 to 2.0.

4.5 Inlet Performance at Take-Off and Approach-to-Landing Conditions

The performance of the inlets was examined for the take-off conditions with a freestream flow of M_0 = 0.3, h_0 = 0 ft, and α_0 = 12 degrees and the approach-to-landing conditions of M_0 = 0.4, h_0 = 5000 ft, and α_0 = 6 degrees. Both conditions required the use of an auxiliary intake to allow addition airflow into the inlet to avoid choked flow conditions within the throat section. The auxiliary intake was formed through the forward translation of a forward section of the cowl which created a gap in the cowl to allow the additional airflow into the inlet. The auxiliary intake can be seen in the left-hand-side images of the inlets in Figs. 20 to 25. This approach for an auxiliary intake is similar to that reported in Ref. [16]. For take-off and approach-to-landing, the forward cowl section was translated forward by Δx = -1.0 ft and Δx = -0.7 ft, respectively, for all inlets. These translations were established through several planar axisymmetric CFD simulations of the M_0 = 1.7 inlet with the auxiliary intake. It was assumed that at these low freestream Mach numbers, the flow within the M_0 = 1.4 and 2.0 inlets behaved in a similar manner as to the M_0 = 1.7 inlet, and so the same cowl translations were used for the M_0 = 1.4 and 2.0 inlets.

For take-off, it is likely that the engine would be operating near full throttle (W_{C2}/W_{C2^*} = 1.0) to provide the thrust needed during take-off. For the M_0 = 1.4 and 1.7 inlets, simulations with $W_{C2}/W_{C2^*} \approx 1$ indicated no choked flow. For the M_0 = 2.0 inlet, choked flow was present within the inlet for $W_{C2}/W_{C2^*} > 0.92$, which means the inlet would limit the possible throttle setting at take-off. Mach number contours on the symmetry planes of the inlets from these CFD simulations are shown in Figs. 20, 21, and 22. With the inlets at an angle-of-attack at α_0 = 12 degrees, the significant features of the flowfields are the sizable, separated regions on the inward surfaces of the windward portions of the forward cowl lips. The boundary layer separation is facilitated by the sharp cowl lips. There is separated flow at the downstream base of the forward cowl segment within the auxiliary intake gap. However, flow does enter the auxiliary intakes and keeps the interior inlet flow from choking. For the M_0 = 1.7 and 2.0 inlets, Figs. 22 and 24 show some local acceleration to supersonic conditions and a localized normal shock on the downstream portion of the cowl.

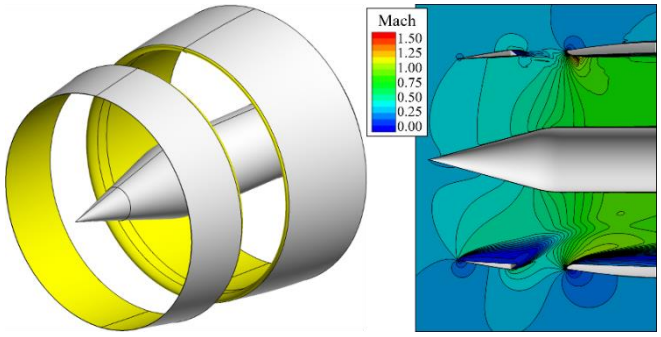

Figure 20. The Mach 1.4 inlet configuration at take-off (left) and Mach number contours on the symmetry plane (right) with W_{C2}/W_{C2^*} = 0.998.

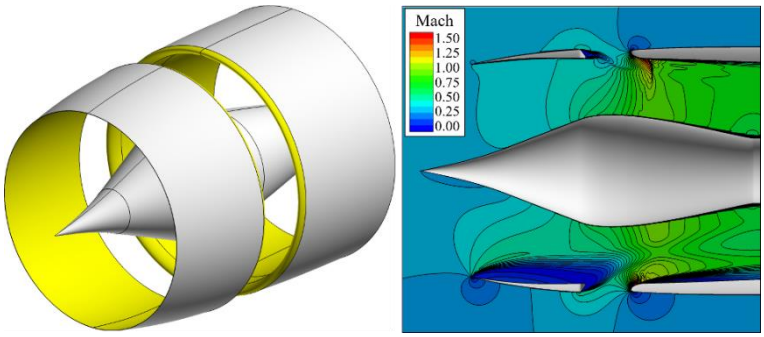

Figure 21. The Mach 1.7 inlet configuration at take-off (left) and Mach number contours on the symmetry plane (right) with W_{C2}/W_{C2^*} = 1.003.

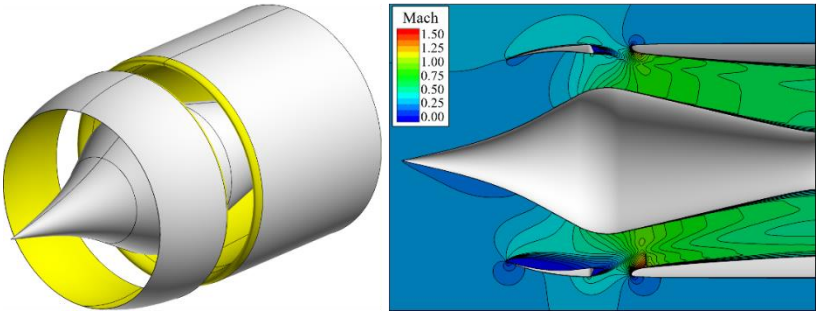

Figure 22. The Mach 2.0 inlet configuration at take-off (left) and Mach number contours on the symmetry plane (right) with W_{C2}/W_{C2^*} = 0.903.

For approach-to-landing, a lower throttle setting of W_{C2}/W_{C2^*} = 0.75 was chosen for examination of the expected flowfields through the inlets. Figures 23, 24, and 25 show images of the Mach number contours at the approach-to-landing conditions for the M_0 = 1.4, 1.7, and 2.0 inlets, respectively. The lower inlet flow rate for the approach-to-landing condition results in lower Mach flow within the inlet; however, the images show separated regions on the windward side on the cowl interior due to the sharp cowl lip and inlet incidence of α_0 = 6 degrees.

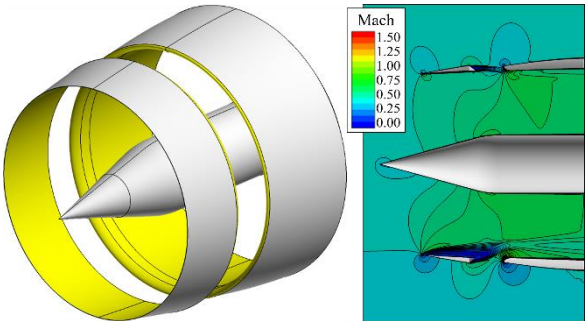

Figure 23. The Mach 1.4 inlet in approach-to-landing configuration (left) and Mach number contours on the symmetry plane (right).

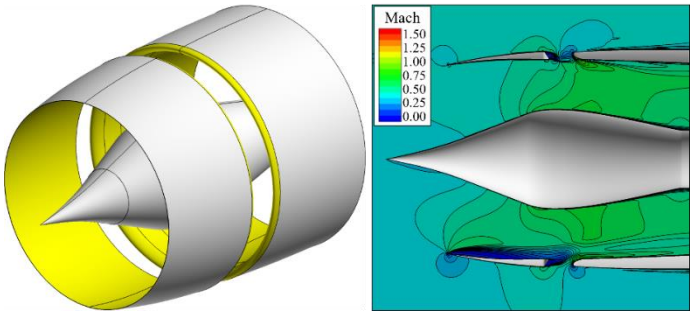

Figure 24. The Mach 1.7 inlet in approach-to-landing configuration (left) and Mach number contours on the symmetry plane (right).

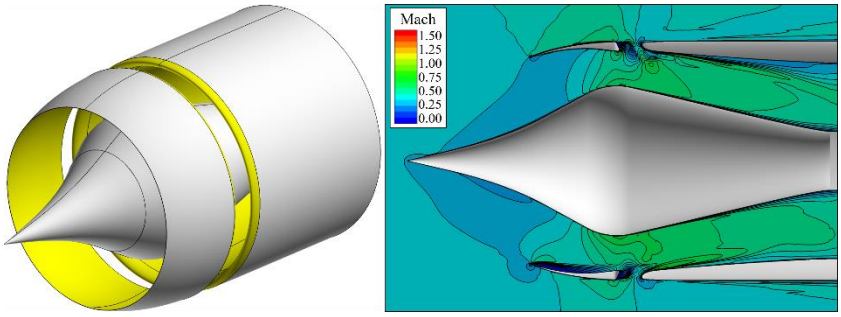

Figure 25. The Mach 2.0 inlet in approach-to-landing configuration (left) and Mach number contours on the symmetry plane (right).

CFD simulations were performed to obtain the characteristics curves for the inlets at both the take-off and approach-to-landing configurations. Those curves are shown in Fig. 26. For the take-off conditions, the total pressure recoveries increase as the freestream Mach number increases from M_0 = 1.4 to 1.7 to 2.0, but the inlet flow ratios decrease. From the images of Figs. 20 and 21, it seems that the M_0 = 1.4 and 1.7 inlets for the take-off conditions have a sizeable separation on the interior surfaces downstream of the auxiliary intake on the windward side of the inlets. This could be a source of losses that reduce the inlet total pressure recoveries. For the approach-to-landing conditions, the total pressure recovery curves for the M_0 = 1.4 and 1.7 inlets are similar. The curve for the M_0 = 2.0 inlet shows similar peak total pressure recoveries, but lower inlet flow ratios. The characteristic curves for the SAE radial total pressure distortion indices are well below the distortion limit, except for the curve for the take-off condition for the M_0 = 1.4 inlet, which is completely above the distortion limit. This seems consistent with the lower inlet total pressure recoveries shown for the M_0 = 1.4 inlet. The inlet performance metrics for the take-off and approach-to-landing conditions are also shown in the plots of Fig. 19 for M_0 = 0.3 and 0.4, respectively.

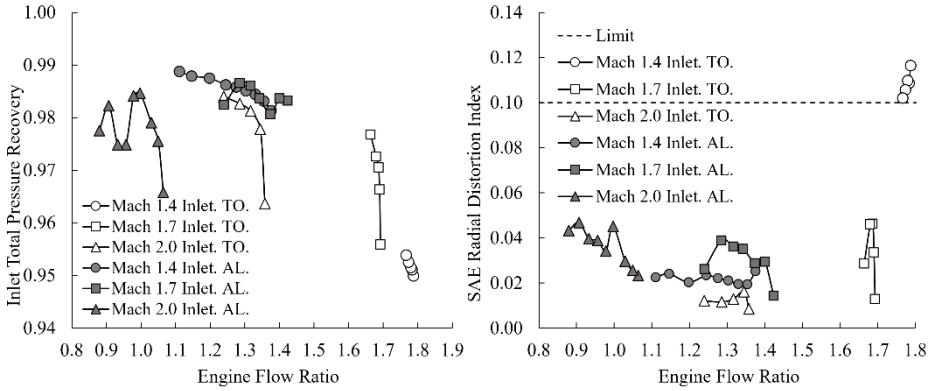

Figure 26. Characteristic curves for total pressure recovery (left) and radial distortion (right) for the inlets at take-off (TO) and approach-to-landing (AL) conditions with use of an auxiliary intake.

5.0 CONCLUSIONS

The design of external-compression, axisymmetric spike inlets for freestream Mach numbers of Mach 1.4, 1.7, and 2.0 were refined and their off-design performance was characterized. The DOE and RSM methods were effective in determining that M_{EX} and r_{cbsh} / h_1 were statistically significant factors for the M_0 = 1.7 and 2.0 inlets and provided guidance on the selection of their optimum values. However, the methods were inconclusive for the M_0 = 1.4 inlet due to excessive noise response as the factors were varied. A further understanding of how to reduce noise is warranted for future studies.

The inlets showed generally good performance at the cruise condition and across the off-design operating conditions. At the cruise condition, the inlet total pressure recoveries exceeded the Mil expectations. In most cases, the total pressure distortion indices were below the suggested limits. Points that exceed the limits involved radial distortion and were mostly at extreme operating ranges of supercritical flow conditions. The inlets performed well for angles-of-attack up to α_o = 5 degrees with acceptable inlet total pressure recoveries and distortion indices well below the limits. Further efforts could be made to refine the M_0 = 2.0 inlet to alleviate the reduction of total pressure recovery and increase in distortion indices during subcritical operation. The use of bleed regions on the centerbody is one possible approach that could be explored further.

The inlets showed mostly acceptable performance for take-off and approach-to-landing conditions with the use of the auxiliary intake formed by the forward cowl translations. The exception was the M_0 = 1.4 inlet for take-off conditions, which showed low total pressure recovery and high radial distortion above the acceptable

limit. Further work is needed to refine the placement and size of the auxiliary intakes for all of the inlets.

Further studies could be performed to examine sensitivities to inlet geometry and performance for different freestream conditions associated with different aircraft missions. The differences would likely be related to changes in the Reynolds number of the flow. A different engine could result in different engine-face Mach numbers, but it is reasonable to expect that advanced, moderate bypass turbofans would have similar engine-face Mach numbers as the engine of the current study.

The inlet designs and performance data provide information on the behaviour of the inlets across the Mach number range from take-off to cruise and could inform the design of inlets for future commercial supersonic aircraft.

ACKNOWLEDGMENTS

The author would like to acknowledge the support of the Commercial Supersonic Technology Project of the NASA Advanced Air Vehicles Program.

REFERENCES

[1] J W SLATER, "Supersonic External-Compression Inlets for Mach 1.4 to 2.0," AIAA-Paper 2023-4016, June 2023.

[2] J J BERTON, D L HUFF, J A SEIDEL, AND K A GEISELHART, "Supersonic Technology Concept Aeroplanes for Environmental Studies," AIAA Paper 2020-0263, January 2020.

[3] SOCIETY OF AUTOMOTIVE ENGINEERS (SAE), "Aircraft Propulsion System Performance Station Designation and Nomenclature," Aerospace Standard (AS) 755, December 1997.

[4] L W HOWERTON and J W SLATER, " Auxiliary Inlet Design Study for Mach 1.4," AIAA Paper 2021-3548, August 2021.

[5] J W SLATER, "SUPIN: A Computational Tool for Supersonic Inlet Design," AIAA Paper 2016-0532, January 2016.

[6] P P WALATKA, P. G. BUNING, L. PIERCE, AND P. A. ELSON, "PLOT3D User's Manual," NASA-TM-101067, March 1990.

[7] D A YODER, "Wind-US User's Guide: Version 4.0," NASA TM 2016-219145, September 2016.

[8] F R MENTER, "Two-Equation Eddy-Viscosity Turbulence Models for Engineering Applications," *AIAA Journal*, Vol. 32, No. 8, pp. 1598-1605, 1994.

[9] SOCIETY OF AUTOMOTIVE ENGINEERS (SAE), "Gas Turbine Engine Inlet Flow Distortion Guidelines," SAE ARP 1420, Rev. C, April 2017.

[10] D N BOWDITCH, R E COLTRIN, B W SANDERS, N E SORENSEN, AND J. F. WASSERBAUER, "Supersonic Cruise Inlets," *Aircraft Propulsion*, NASA SP-259, November 1970.

[11] S M HIRT, R V CHIMA, M A VYAS, T R CONNERS, T R WAYMAN, AND R W REGER, "Experimental Investigation of a Large-Scale Low-Boom Inlet Concept, " AIAA Paper 2011-3796, June 2011.

[12] D C MONTGOMERY, Design and Analysis of Experiments, 5th Edition, John Wiley and Sons, New York, 2001.

[13] MIL-STD-5007E, "Engines, Aircraft, Turbo-Jet, and Turbofan, Model Specifications For," September 1983.

[14] W G STEENKEN, J G WILLIAMS, A J YUHAS, AND K R WALSH, "An Inlet Distortion Assessment during Aircraft Departures at High Angle of Attack for an F/A-18A Aircraft," NASA TM-104328, March 1997.

[15] PRATT & WHITNEY AND GENERAL ELECTRIC AIRCRAFT ENGINES, "Critical Propulsion Components, Volume 4: Inlet and Fan/Inlet Acoustics Team," NASA CR 213584, Vol. 4, May 2005.

[16] G A GARZON, "Use of a Translating Cowl on a SSBJ for Improved Takeoff Performance," AIAA Paper 2007-0025, January 2007.